RESEARCH ARTICLE

VOLCANICA

Alkali activated materials from Tajogaite volcanic ash (La Palma, Spain): a green recovery after the 2021 eruption

Roberta Occhipinti[α], Silvia Portale[α,β], Gabriele Lanzafame*[α], Domingo Gimeno[γ], Marko Kudrna Prašek[δ], Paolo Mazzoleni[α], and Germana Barone[α]

[α] Dipartimento di Scienze Biologiche, Geologiche e Ambientali, Università degli studi di Catania, Italy.
[β] Dipartimento di Scienze Umanistiche, Università degli studi di Catania, Italy.
[γ] Departament de Mineralogia, Petrologia i Geologia Aplicada, Facultat de Ciències de la Terra, Universitat de Barcelona, Spain.
[δ] Elettra-Sincrotrone Trieste S.C.p.A., Basovizza (Trieste), Italy.

Abstract

The 2021 Tajogaite eruption was marked by intense pyroclastic fallout that covered a substantial portion of La Palma island, with maximum thicknesses in the central-western part. This, combined with lava flows, resulted in widespread damage to public and private properties. In this study, we investigated if volcanic ash from this eruption could serve as a raw material in the synthesis of alkali activated materials (AAMs) and contribute to the construction of eco-friendly buildings and the restoration of those damaged by the eruption. Volcanic ash-based AAMs were synthesized using NaOH and Na_2SiO_3 as alkaline solutions and by adding metakaolin to enhance ash reactivity and enable processing at ambient temperatures. Lightweight porous AAMs were also produced using H_2O_2 and metallic aluminum as foaming agents. Chemical, textural, physical, and mechanical analyses on the final products assessed their suitability as environmentally friendly materials to be used in the reconstruction of the island infrastructure, opening new perspectives on recovery actions that can be undertaken after disastrous eruptions. Of all the islands in the Canary Archipelago, La Palma has experienced the highest number of eruptions (8) in historical times, all of which showing considerable similarity in terms of eruptive mechanisms and composition to the most recent Tajogaite event. Although this study investigated fresh Tajogaite ash, similar perspectives can be envisaged for both other recent eruptions at La Palma and other similar volcanic scenarios worldwide.

Keywords: Volcanic Ash; Tajogaite; Alkali activated materials; Recovery; Green economy.

Submitted: 2024-01-24 | Accepted: 2024-08-11 | Published: 2024-10-06

Editor: U. Kueppers | Typesetter: J. Farquharson

1 Introduction

After 50 years of quiescence, Tajogaite volcano, located on La Palma Island (Canary Archipelago, Spain), began its most recent eruption on 19th September 2021 with the opening of two 200 m-long fractures [Longpré 2021] on the western flank of the Cumbre Vieja ridge at 840–1100 m above sea level (a.s.l.) in the municipality of El Paso. The effects of this 85-day-long eruption had wide resonance worldwide due to the damage caused to the surrounding areas and population as a result of ash fallout and lava flow invasion, forcing the evacuation of ~8000 residents and leading to the loss of 2800 buildings and 100 hectares of plantations worth more than 800 million euros [Longpré 2021; Carracedo et al. 2022]. The eruption was characterized by lava fountaining, Strombolian activity, and frequent ash emission frequently emitting considerable amounts of volcanic ash [Romero et al. 2022b], which constructed the 200 m-high Tajogaite cinder cone in the earliest and main stages of the eruption [Civico et al. 2022; Ruggieri et al. 2023, and references therein]. Emissions of low-viscosity basanitic lavas [Castro and Feisel 2022] and tephra alternated and overlapped throughout the eruption, with lavas that rapidly flowed towards the inhabited areas of El Paraíso, Todoque, and El Pedregal, reaching the sea in 10 days [Carracedo et al. 2022] (Figure 1). The eruption had a Volcanic Explosivity Index = 3, producing ash columns mostly between 1.6 and 2.7 km in height above the vents, with a peak of 8 km in the final stage of eruptive activity [Romero et al. 2022b]. During explosive activity, volcanic ash forms in the upper portion of a volcano feeding system when magma fragments and pyroclasts are ejected into the atmosphere [Dingwell et al. 2012]. Small fragments may cool sufficiently quickly to avoid complete crystallization, producing clasts with abundant glassy groundmass. During the 2021 Tajogaite eruption, a total amount 45×10^6 m^3 of tephra was discharged into the atmosphere [Carracedo et al. 2022] with a peak ejection rate of ~18 m^3 s^{-1} [Romero et al. 2022a; b]. Although the ash deposit isopach contours were elongated NE–SW [Romero et al. 2022a], the pyroclastic fallout affected many areas of the La Palma Island, with deposit thickness varying between 3 mm and 1.2 m from 13.5 to 1.1 km in distance [Romero et al. 2022a]. The large amount of tephra fallout had a serious impact on the economic activities (including touristic ones) of the entire island, since it affected different sectors of society and infrastructure, e.g. causing severe damage to agricultural production, destruction of roads, and flight cancellations. Besides the immediate aftermath of pyroclast emission and fallout, long-term impacts include risks to human and animal health related to air quality and water contamination [Horwell and Baxter 2006; Stewart et al. 2006; Barone et al. 2021; Ruggieri et al. 2023].

Therefore, an urgent need arises for swift clean-up operations in order to avoid respiratory and ingestion hazards and to restore functionality to both rural and urban environments. This, in turn, leads to the necessity of disposing of and storing

* gabriele.lanzafame@unict.it

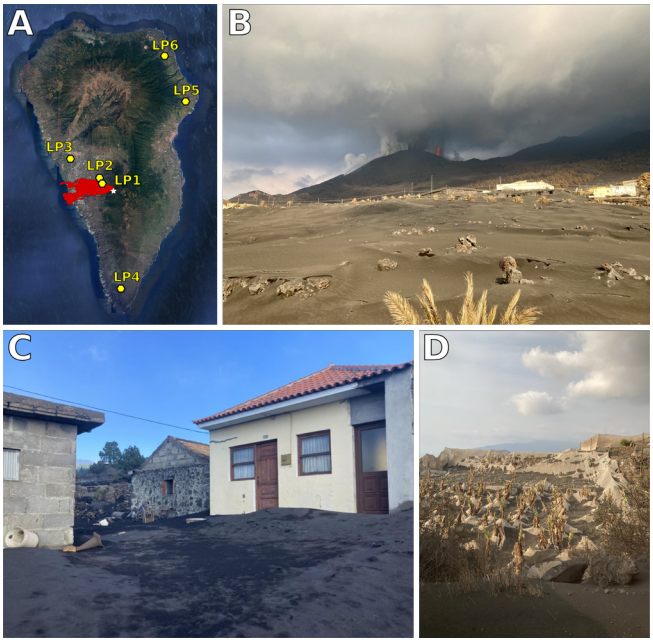

Figure 1: [A] sampling locations and lava field of the 2021 eruption; [B] Explosive activity of Tajogaite crater seen from El Paso municipality (December 2021). Aftermath of tephra fall on villages [C] and cultivated areas [D].

the removed ash in specific landfills and adopting strategies for its potential re-use.

One of the most promising approaches to addressing these issues is the transformation of volcanic ash from waste to resource. Volcanic clasts > 63 μm can be potentially used as light aggregates for mortars, concrete, plasters, and ceramics in order to provide a structural support for the finished product, while the finer fraction (< 63 μm) has features ideal for its use as filler (i.e. a fine material, often inert, added to cement or concrete to improve its properties), aimed at reducing the porosity of the paste (the mixture of cement and water that binds aggregate particles in concrete) and improving its mechanical properties. Recently, both fresh and old volcanic ash has been exploited as a natural resource in the production of sustainable and innovative "cement-free" materials known as alkali activated materials (AAMs) in various geographic contexts with past or presently active volcanism (Colombia, Democratic Republic of Congo, Indonesia, Italy, Russia, and United States) thanks to its *pozzolanic* properties whereby, despite having few or no cementitious properties on its own, volcanic ash can undergo chemical reactions to form cementitious compounds [Tchakoute Kouamo et al. 2012; Tchakoute et al. 2013; Djobo et al. 2017; Finocchiaro et al. 2020; Barone et al. 2021; Játiva et al. 2021; Lemougna et al. 2021; Occhipinti et al. 2022; 2023a; b]. AAMs can be prepared without any thermal treatment by mixing powdery aluminosilicate materials (precursors) with an alkaline solution, such as NaOH and $NaSi_2O_3$ (activators). The alkaline attack allows the aluminosilicate chains of the precursor to break down and reorganize into an amorphous gel through a polycondensation mechanism [Davidovits 1991]. After curing process (i.e. the process of setting and hardening of the paste), the gel takes on the appearance of a cement and the final product shows good performance in terms of mechanical strength, chemical stability and heat resistance [Provis and van Deventer 2009].

The versatility and adaptability of AAMs lies in the nature of the raw materials. Indeed, AAM technology exploits a wide range of aluminosilicate sources as precursors with different availabilities, reactivities, costs and value in different geographic contexts. In past decades, AAMs were developed and promoted as components of a "sustainable" cement-based system for the future. The feasibility of transforming industrial by-products (e.g., fly ash) or natural materials into resources through alkali activation processes offers a green alternative to traditional cement-based materials, whose manufacturing process contributes to approximately 10 % of global CO_2 emission into the atmosphere [Shi et al. 2019; Belaïd 2022]. The precursors utilized in alkali activation technology can have various origins, from industrial waste (i.e. fly ash, metallurgical slag, glass waste and residues of mining activity) [e.g. Bernal et al. 2016; Matinde 2018; Occhipinti et al. 2021] to natural raw materials [e.g. Clausi and Pinto 2023]. Among the latter, mafic volcanic ash has proven particularly suitable in promoting alkaline activation because of its comparably high bulk Al- and Si-content and the presence of volcanic glass. Recently, basaltic to trachybasaltic ash from Mt. Etna volcano (Sicily, Italy) was successfully used as precursor in the production of AAMs [Finocchiaro et al. 2020; Barone et al. 2021; Occhipinti et al. 2022; 2023a; b]. AAMs made with volcanic ash with an alkali-basaltic composition show good polymerization (extent of the three-dimensional development of the polymeric gel), mechanical strength, durability, and versatility, and have been proposed both for use as a construction material and, more recently, for restoration purposes [Barone et al. 2021; Fugazzotto et al. 2023; Portale et al. 2023].

During and after the 2021 Tajogaite eruption, a substantial amount of volcanic ash from roads and residential areas was collected and stored in containers arranged in city disposal areas. Treated as waste, this natural product was therefore devalued and destined for landfill or simply thrown into the sea. In this study, different kind of AAMs were produced using Tajogaite volcanic ash and investigated as potential green construction and restoration materials. If suitable, they could contribute to the reconstruction of infrastructure. Recent attempts by Tashima et al. [2023] and Mañosa et al. [2023] demonstrated that Tajogaite volcanic ash can be properly used as a raw material in the preparation of AAMs after curing at temperatures in the range of 40 to 85 °C for several hours. Working at these temperatures increases the reactivity of the ash, ensuring good mechanical properties [Djobo et al. 2017]. However, such a process is expensive and requires large amounts of energy as well as specific equipment such as ovens, which are not commonly available in situ (e.g. on the construction site) and can only be used in the production of pre-casted materials. In this regard, the main focus of this study is to avoid any thermal curing treatment, obtaining products that can be synthesized directly on-site.

Alkali activated materials (binder and porous types) were developed and tested (Figure 2 and Table 1). Binders can

Table 1: Details of AAM mix design expressed as wt.% of the total slurry.

Samples	Ash (wt. %)	MK (wt. %)	NaOH (wt.%)	Na_2SiO_3 (wt.%)	H_2O (wt.%)	H_2O_2 (wt.%)	Al (wt.%)	L/S*
LP0	80.6	-	19.4	-	-	-	-	0.2
LP0-NaOH-Na_2SiO_3	79.0	-	10.5	10.5	-	-	-	0.3
LP10-NaOH	71.7	8.0	20.3	-	-	-	-	0.3
LP20-NaOH	61.4	15.4	23.2	-	-	-	-	0.3
LP10	68.2	7.6	4.6	14.4	5.3	-	-	0.3
LP20	60.6	15.2	4.6	14.4	5.3	-	-	0.3
LP10-P	64.3	7.2	4.3	13.6	5.0	5.7	-	0.3
LP10-Al	67.9	7.5	4.5	14.3	5.3	-	0.4	0.3
LP20-P	57.2	14.3	4.3	13.6	5.0	5.7	-	0.3
LP20-Al	60.4	15.1	4.5	14.3	5.3	-	0.4	0.3

* L/S = liquid to solid ratio includes all the solution and water.

Table 2: Major oxide composition of volcanic ash (wt.%) and crystal composition of volcanic ash and AAM binders. Ant = anatase; Aug = augite; Fo = forsterite; Mag = magnetite; Ms = muscovite; Pl = plagioclase; Qz = quartz; Tnat = thermonatrite.

	Volcanic ash						AAMs	
Sample	LP1	LP2	LP3	LP4	LP5	LP6	LP10	LP20
	X-ray fluorescence							
SiO_2	44.54	44.38	44.41	44.82	44.87	44.99	n.a.	n.a.
TiO_2	3.60	3.62	3.79	3.67	3.71	3.72	n.a.	n.a.
Al_2O_3	13.48	13.47	14.29	15.63	15.10	15.17	n.a.	n.a.
FeO	12.20	12.26	12.40	11.57	11.84	11.88	n.a.	n.a.
MnO	0.19	0.19	0.20	0.20	0.20	0.19	n.a.	n.a.
MgO	8.67	8.61	7.37	5.70	6.32	6.25	n.a.	n.a.
CaO	11.31	11.33	11.20	9.90	10.45	10.46	n.a.	n.a.
Na_2O	3.63	3.67	3.89	4.83	4.31	4.41	n.a.	n.a.
K_2O	1.44	1.43	1.56	1.94	1.76	1.77	n.a.	n.a.
P_2O_5	0.75	0.75	0.84	1.06	0.86	0.86	n.a.	n.a.
Tot	99.82	99.73	99.94	99.32	99.43	99.69	n.a.	n.a.
	X-ray diffraction							
Ant	n.a.	-	n.a.	n.a.	n.a.	n.a.	-	1.8 (± 0.03)
Aug	n.a.	25.1 (± 1.3)	n.a.	n.a.	n.a.	n.a.	18.9 (± 0.9)	15.6 (± 0.7)
Fo	n.a.	9.4 (± 0.5)	n.a.	n.a.	n.a.	n.a.	4.9 (± 0.03)	4.5 (± 0.2)
Mag	n.a.	2.2 (± 0.1)	n.a.	n.a.	n.a.	n.a.	0.1 (± 0.02)	0.03 (± 0.03)
Ms	n.a.	-	n.a.	n.a.	n.a.	n.a.	11.2 (± 0.7)	11.19 (± 0.7)
Pl	n.a.	12.1 (± 0.9)	n.a.	n.a.	n.a.	n.a.	10.6 (± 0.8)	8.2 (± 0.4)
Qz	n.a.	-	n.a.	n.a.	n.a.	n.a.	0.4 (± 0.04)	1.5 (± 0.1)
Tnat	n.a.	-	n.a.	n.a.	n.a.	n.a.	1.8 (± 0.2)	1.0 (± 0.1)
Amorphous	n.a.	51.3 (± 3.7)	n.a.	n.a.	n.a.	n.a.	52.7 (± 2.4)	60.2 (± 1.8)
Total	-	100	-	-	-	-	100	100

be used in the construction and restoration fields [Clausi et al. 2016; Barone et al. 2020; Occhipinti et al. 2020], whereas porous AAMs can be used in a wide range of applications including adsorbents [Ge et al. 2015; Bhuyan et al. 2022], catalysts or catalyst supports [Alzeer et al. 2016; Alzeer and MacKenzie 2018; Clausi and Pinto 2023], thermal [Feng et al. 2015] and acoustic insulation [Zhang et al. 2015; Luna-Galiano et al. 2018], fire-resistant materials [Rickard et al. 2013; Rickard and van Riessen 2014], and pH regulators [Novais et al. 2018; Vitola et al. 2020]. A multidisciplinary approach allowed us to fully characterize both the chemical and textural features of the starting material and the mechanical and physical properties of the resulting AAMs. Results indicate that this approach could represent a potential solution to the issue of the volcanic ash accumulation and thus lead to a reduction in waste disposal costs. Indeed, the transformation of waste materials into resources forms part of the virtuous mechanism within a circular economy, leading to a more limited exploitation of virgin

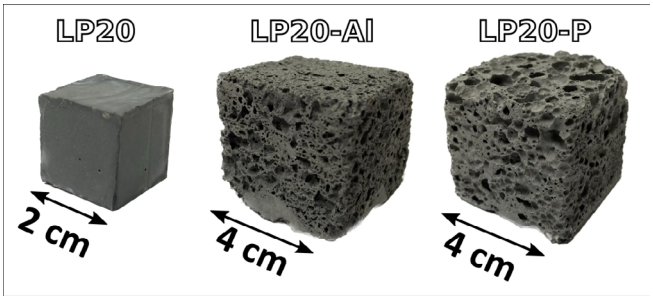

Figure 2: Binders and porous AAMs based on Tajogaite ash at hand-scale after 28 days of room temperature curing.

resources and promoting the use of local materials. Additionally, the possibility of creating highly versatile materials suitable for green construction practices and adaptable to many fields of application opens up the way for the widespread adoption of alternative technologies and innovative processes in the construction and manufacturing industries.

2 Methods and materials

2.1 Raw materials

The sampling campaign was performed during the last phase of the Tajogaite eruption, in mid-December 2021. Ash was sampled at six different localities of the island at increasing distances from the eruptive centre. LP1 and LP2 were collected close to the eruptive vent, LP5 and LP6 at the greatest distance (Figure 1A). Specifically, LP1 to LP4 were collected from natural deposits (Figure 1B–D), while LP5 and LP6 were collected from waste bins set up by the authorities in different inhabited areas around the island, with the purpose of further disposal. Consequently, in addition to the material naturally ejected by the volcano, dirt of organic and inorganic nature is found in these two samples. Among the natural deposits (LP1-LP4), cleaner in terms of extraneous particulate matter, LP2 was chosen as a precursor for AAM preparation. It is worth noting that this ash should not be considered strictly pristine, since between emission and collection, it had been subjected to weathering that may have leached out soluble elements.

All samples were dried for 24 hours at 100 °C to remove moisture and then mechanically milled using an agate jar stirrer in order to obtain a powder with particle size < 50 µm.

2.2 Alkali activated products

In order to assess the reactivity of the sole raw material through the alkaline activation process, ash was activated with NaOH (8 M) and NaOH/Na_2SiO_3 solutions. The formulations were defined on the basis of the liquid to solid (alkaline solution/precursor) ratio. This ratio is crucial in achieving optimal workability in the production of AAMs and plays a significant role in both the mixture consistency and ease of handling during application. Next, in order to improve the reactivity of the ash while avoiding any thermal curing or an increase in the alkalinity of the activators, a small percentage of commercial metakaolin (*MK, ARGICAL™ M - 1000, Imerys*, France, a high reactive aluminosilicate source) was added to the ash (refer to Davidovits et al. [1999] and Gimeno et al. [2003] forthe explanation of this procedure), following the well-established procedure tested for the formulation of AAMs using basaltic Etnean ash [Barone et al. 2020; Finocchiaro et al. 2021; Occhipinti et al. 2022; 2023a; b].

Alkaline activators used in this study were 8 M sodium hydroxide (*Carlo Erba reagents s.r.l.*, Italy) and sodium silicate (molar ratio SiO_2/Na_2O = 2 *Ingessil s.r.l.*, Italy). Tap water, sourced from Etnean groundwater, was added to all formulations to transform the pastes from sticky to workable and to mitigate the alkaline conditions of the operational procedure. Solid precursors were mixed with the alkaline solution by mechanical stirring for 3 min. The slurry was then poured into moulds and vibrated for 60 seconds to remove the air bubbles formed during the mixing. Finally, porous alkali activated materials were also produced in separate experiments by adding a well-defined percentage of hydrogen peroxide or metallic aluminum directly to the slurries. These foaming agents are capable of an in-situ generation of gas which becomes trapped during the hardening of the pastes [Bai and Colombo 2018; Novais et al. 2020; Zhang et al. 2021]. Before any physical-chemical characterization took place, all samples were cured at room temperature for 28 days in a sealed vessel. All the details of formulations are reported in Table 1.

2.3 X-ray Fluorescence (XRF)

Concentrations of major elements of volcanic ash were determined by wavelength dispersion X-ray fluorescence at CCiT-UB (Centres Científics i Tecnològics de la Universitat de Barcelona) by means of a wavelength dispersive X-ray fluorescence spectroscope (WDXRF), Panalytical, Axios PW 4400/40 sequential spectrophotometer. Powdered samples were conserved overnight in an oven at 90 °C in an open glass beaker. Next, 0.3 g of powder was mixed with lithium tetraborate of pure analytical grade in a 1:20 ratio and homogenized with a glass bar before being placed inside of a Pt crucible. Three drops of lithium iodide were added to the mix in order to obtain a good correction of the mix prior to melting, following which the crucible was placed inside the refractory cup of an induction kiln and melted at 1400 °C in a heating cycle lasting 15 minutes. Finally, the incandescent liquid was poured into a flat Pt dish in order to obtain a glassy homogeneous pearl with an ideal analytical flat surface, and cooled in a two-minute cycle in order to avoid crystallization of the pearl. This was repeated three times with each sample. International reference standards JA-3 and JB-3 kindly provided by the Geological Survey of Japan were repeatedly measured as unknown to monitor precision and accuracy. For major elements, analytical precision (1σ, n = 12) was 2 % or better [Gisbert and Gimeno 2017] except for Na at values lower than 2.5 % of Na_2O, but this poorer precision was controlled systematically in-house through ICP-OES analysis (see Aulinas et al. [2010] for procedures). Loss on ignition (LOI) in an oxidizing environment furnace (see Lechler and Desilets [1987] for implications) was not determined since most of the iron present in the samples is in a reduced for and due to the extremely pristine nature of the samples. The XRF device was

calibrated using international rock standards (see Gisbert and Gimeno [2017] for a detailed procedure).

2.4 X-Ray Diffraction (XRD)

XRD measurements were performed on both raw materials and AAMs by using a Miniflex Rigaku X-ray powder diffractometer, equipped with Ni filter Cu Kα radiation generated at 40 kV and 15 mA. The measurement was set at a scanning speed of 5.0° min^{-1}, step of 0.0200° within the range of 5 to 65°, for a duration of 14 minutes per sample. Qualitative analysis was performed via the search/match technique using `Profex 5.0.0` software, while quantitative analysis of crystalline and amorphous phases was carried out using the Rietveld method and corundum as an internal standard [Gualtieri and Zanni 1998].

2.5 Fourier Transform Infrared Spectroscopy (FT-IR)

FT-IR analyses were performed using a Thermo Fisher Scientific Nicolet 380 infrared spectrometer in the Attenuated Total Reflection (ART) mode. The powered samples were placed onto a diamond support and all measurements were carried out at room temperature. The spectra wavelength ranges between 400 and 4000 cm^{-1}, with a resolution of 4 cm^{-1}. Results were collected using `Omnic` software.

2.6 Scanning Electron Microscopy (SEM-EDX)

Back-scattered electron (BSE) images and chemical analyses were performed on both carbon coated volcanic ash and AAMs by means of a Tescan Vega-LMU Scanning Electron Microscope equipped with an EDAX Neptune XM4-60 microanalyzer operating by energy dispersive system. The microanalyzer is characterized by an ultrathin Be window coupled with an EDAX WDS LEXS (wavelength dispersive low energy X-ray spectrometer) calibrated for light elements. Operating conditions were set at 20 kV accelerating voltage and approx. 8 nA beam current for obtaining high resolution BSE images and 20 kV accelerating voltage and 0.2 nA beam current for analysing major element abundances.

2.7 pH and electrical conductivity

pH and electrical conductivity were evaluated by dipping a cubic sample of each formulation into beakers filled with double-distilled water using a weight ratio of 1:10. The measurements were taken at 0, 15, 30, 60, 120, 720, and 1440 minutes after immersion for a total testing time of 24 h [Barone et al. 2021]. The pH was measured using a pH/mV/Temp Meter Eurotek by ORMA calibrated on solutions at pH 4.01, 7, and 9.18. Data on electrical conductivity was collected using an Orion Portable Conductivity Meter model 150.

2.8 Synchrotron Radiation X-ray microtomography (SR μCT) and 3D image analysis

The study of 3D texture and pore phase of the 6 AAF samples was performed by high-resolution SR μCT in phase-contrast mode [Cloetens et al. 1997]. The experiments were carried out at the SYRMEP beamline of the Elettra - Sincrotrone Trieste laboratory in Basovizza (Trieste, Italy). Samples with a regular shape (size of ~4 × 4 × 8 mm) were illuminated by a filtered (1.5 mm Si + 1.0 mm Al) polychromatic X-ray beam delivered by a bending magnet source in transmission geometry. The resulting mean X-ray energy was of approximately 27 keV. For each sample, 1800 radiographs (projections) were acquired at a sample-detector distance of 150 mm, with an exposure time of 1 s per projection and an effective pixel size of the detector set to 2.4 × 2.4 μm, yielding a maximum field of view of approx. 4.91 × 4.91 mm. The detector used was an air-cooled, 16 bit, sCMOS camera (Hamamatsu C11440-22C) with a 2048 × 2048 pixel chip. Reconstruction of tomographic slices was performed using the Syrmep Tomo Project (STP) software suite [Brun et al. 2017], applying a single-distance phase-retrieval algorithm based on the Transport of Intensity Equation (TIE) [Paganin et al. 2002] to the sample projections. The 3D processing and analysis of the microtomographic images were performed by `Fijii` freeware software [Schindelin et al. 2012] and `pyPore3D` software library developed at Elettra [Aboulhassan et al. 2022]. Using `Fijii`, Volumes of Interest (VOIs) corresponding to a size of about 12–14 mm^3 (Figure 5 and Supplementary Material 1 Table S1) were extracted from each image stack, filtered by a mean filter in order to remove noise and manually segmented to isolate the sole pore phase. Binary images were then processed by `pyPore3D` applying a cycle of erosion and dilation in order to remove outlying background objects of < 3 voxels. On these images, quantitative investigations were performed following the procedures described in Lanzafame et al. [2020] in order to calculate the samples' porosity and the morphological characteristics (volume, sphericity, aspect ratio) of each pore. The degree of connectivity of the pore network, expressed by the connectivity density parameter [Brun et al. 2010], was determined by a skeletonization approach, using the LKC algorithm [Brun et al. 2010]. The 3D visualization of the reconstructed and processed images was performed by volume rendering procedures using the commercial software `VGStudio MAX 2.0` (Volume Graphics).

2.9 Mechanical strength tests

Flexural and compressive strength tests were performed on samples after 28 days of curing by means of a 70-T1182 UNIFRAME (Controls) automatic compression testing machine. The three-point bending test was performed on sets of three prisms per formulation (2 × 2 × 8 cm) according to UNI EN 1015-11: 2019. This allowed an assessment of the AAMs' flexural strength via the application of increasing stress operated by a 10 kN load cell at a rate of 20 N s^{-1}. Following the flexural test, the obtained half prims were subject to compressive strength according to UNI-EN 1015-11: 2019. Each specimen was tested by means of a 50 kN gauge load cell at a rate of 1200 N/sec until the maximum bearable stress was reached. Measurements were collected by `RTM Terminal` software.

3 Results

3.1 Volcanic precursor characterization

Bulk rock analysis performed on the volcanic ash employed as a precursor revealed an Ocean Island Basalt (OIB) composi-

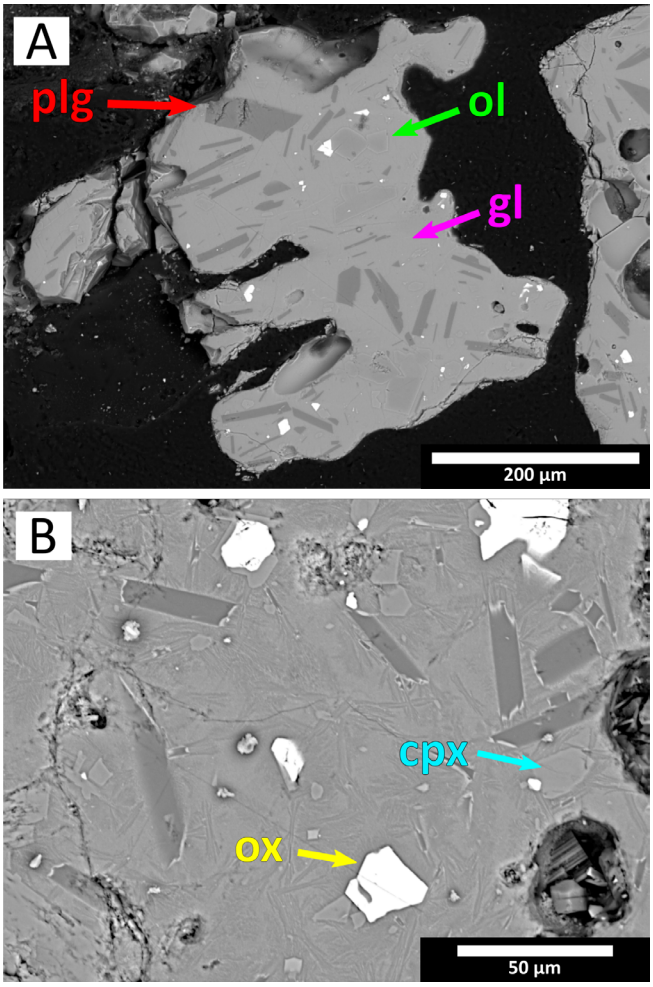

Figure 3: Electron back-scattered images of two ash grains from Tajogaite 2021 eruption displaying texture made of small crystals of plagioclase (plg), olivine (ol), clinopyroxene (cpx) and Ti-Fe oxides (Ox) in [A] glassy (gl) and [B] cryptocrystalline groundmass. The cryptocrystalline matrix displays dendritic crystals (micrometric to sub-micrometric) grown under high cooling rates during the solidification of the sample in the air.

tion, confirming previous studies reported in literature for the 2021 eruption tephra and lavas [Pankhurst et al. 2022; Romero et al. 2022a; González-García et al. 2023]. The volcanic ash falls in the basanite field of the Total Alkali vs. Silica diagram [Le Maitre 2002] (Supplementary Material 1 Figure S1) with a range of SiO_2 = 44.43–45 wt.%, Al_2O_3 = 13.50–15.74 wt.%, MgO = 5.73–8.68 wt.%, and Na_2O+K_2O = 5.07–6.81 wt.% (Figure 2). SEM-BSE images (Figure 3) show that ash grains, with a size of about one millimetre, have a very irregular shape, a generally aphanitic structure with a hypocrystalline texture containing a low amount of tiny (up to 200 µm) crystals of plagioclase ($An_{46–61}$), diopside and augitic clinopyroxene, olivine (Fo80–84) and Ti-Fe oxides, with euhedral to subhedral habitus. The groundmass, when not completely hyaline, can be either microcrystalline or cryptocrystalline. SEM micro-chemical analyses of samples LP1, LP2, and LP5 reveal a slight increase in the alkali and silica content of the glass with respect to the whole-rock (Supplementary Material 1 Figure S1) with a composition shifted towards phono-tephrite. XRD analysis results (Supplementary Material 1 Figure S2) display detected peaks attributable to the same crystalline phases described above plus a consistent amorphous phase due to the glassy nature of the ash. Quantitative calculation confirms the typical assemblage of OIB alkaline products given by crystals of plagioclase and pyroxene (20.20 wt.% and 20.78 wt.%, respectively), followed by olivine (7.72 wt.%) and iron oxides (2.42 wt.%). The amorphous phase reaches values higher than 46 wt.%. FT-IR spectra in Attenuated Total Reflection (ATR) mode of the investigated ash (Supplementary Material 1 Figure S3) show a main broad band characterized by two shoulders, one at 960 cm^{-1} and the other at 906 cm^{-1}. According to available literature, the area between 900 and 1200 cm^{-1} is attributable to Si-O-T vibration (where T = Si or Al) [Rees et al. 2007], thus indicating the occurrence of aluminosilicate materials. Moreover, low intensity bands around 750–790 cm^{-1} are attributable to the ring vibration of Si-O bonds [Sitarz et al. 2000]. A small band in the area of 675 cm^{-1} is attributable to the stretching vibration of Al-O bonds when the aluminum ions are in fourfold coordination [Clayden et al. 1999].

Characterization of alkali activated materials

A first series of mixtures of only Tajogaite ash and alkaline activators, i.e. NaOH (8 M) and NaOH/Na_2SiO_3 for samples LP0 and LP0-NaOH-Na_2SiO_3 (where LP0 corresponds to a mixture of ash and NaOH and LP0-NaOH-Na_2SiO_3 also includes the addition of Na_2SiO_3, see Table 1), respectively, was prepared at room temperature in order to test the simplest possible system. Nevertheless, the tested formulations did not harden within 72 hours at room temperature and did not show chemical-physical stability due to the low volcanic ash reactivity in such alkaline conditions. Therefore, formulations with 10 and 20 wt.% of metakaolin (LP10-NaOH and LP20-NaOH, respectively, where '10' and '20' refer to the metakaolin content, see Table 1) were tested using at first only 8 M NaOH. Although the pastes hardened within 72 hours, they did not adequately strengthen, appearing very brittle. Good results were obtained when an amount of 14.4 wt.% (over the total weight of the paste) of Na_2SiO_3 was added to the NaOH solution (LP10 and LP20, see Table 1). In this work, only the binders which developed strength after 24 hours (LP10 and LP20) were selected and then investigated after 28 days in order to study their mineralogical, microstructural, physical, and mechanical features. These formulations were then used as binders to prepare porous AAMs.

The mineralogical composition of the obtained binders is reported in Table 2. Both samples LP10 and LP20 show the same mineral phases of the original ash except for the presence of quartz, muscovite and anatase, which derive from metakaolin. All binders show a signal related to the amorphous aluminosilicate gel [Barbosa et al. 2000; Rowles and O'Connor 2003; Fletcher et al. 2005], recognizable by a slight halo between 20 and 35° 2θ. Peaks related to the occurrence of thermonatrite ($Na_2CO_3 \cdot H_2O$) were detected at 2θ values of 33.8, 38.2, 45.5°, even though there are no visible efflorescences on the surface of the samples which generally form by salts precipitation due to an excess of Na^+ reacting with atmospheric CO_2.

Quantitative analyses of the mineralogical and amorphous phases were carried out through the Rietveld method [Gualtieri and Zanni 1998] (Table 2). As expected, both binders show an increase in the amorphous phase with respect to the starting material (LP10 Amorph = 59.86 wt.%; LP20 Amorph = 67.47 wt.%; Ash Amorph = 46.88 wt.%). We observed a positive correlation between the amorphous content and the amount of metakaolin added, and a negative correlation between the amount of metakaolin added (LP20) and thermonatrite occurrence. In terms of nature and amount of constituent minerals, no significant differences were detected by XRD patterns in the porous samples compared to the binders.

FTIR-ATR analyses of LP10 and LP20 binders and of the corresponding porous samples (LP10-P, LP10-Al and LP20-P, LP20-Al with peroxide and aluminum as foaming agents, respectively) are shown in Supplementary Material 1 Figure S3. Overall, the position of the main absorption band related to anti-symmetric Si-O (Al) stretching vibrations is detected in the range of 970 cm^{-1}, which is shifted to higher wavenumbers with respect to the original volcanic ash precursor (960 cm^{-1}). The shoulder at 888 cm^{-1} is visible in the ash spectrum and attributable to the presence of insoluble crystalline anorthite or diopside [Taylor 1990] from the original raw material. These crystals do not take part in the reaction [Tashima et al. 2023]. This shoulder appears shifted towards lower wavenumbers (i.e. 867 cm^{-1} for LP10, LP10-P and LP20, LP20-P and 864 cm^{-1} for sample LP10-Al and LP20-Al) as a consequence of the Al-OH stretching vibration [Hajimohammadi et al. 2017; Occhipinti et al. 2023b] or of the Si-OH bending vibration, indicating that structural modification has occurred. Furthermore, Al-O bond vibration determines less intense bands found at 675 cm^{-1} and 692 cm^{-1}. Finally, two new bands were detected at 1263 cm^{-1} and at 795 cm^{-1} for the samples LP10-Al, LP20-P and LP20-Al. These bands can be attributed to the stretching vibration of (Si, Al)–O and O–Si–O respectively [Razak et al. 2014; Lemougna et al. 2021]; however, they are more pronounced in the sample with 20 wt.% metakaolin and in the presence of aluminum. A signal at 1400 cm^{-1} occurs in all the spectra and is determined by the stretching vibration of $(CO_3)^{-2}$ [Pathak et al. 2008]. This may denote the presence of carbonates formed with the contribution of atmospheric CO_2 [Criado et al. 2005] while those at 1650 cm^{-1} and 3350–3390 cm^{-1} can be attributed to the vibration of H-O-H and OH bonds due to the presence of tap water used for the formulation during the preparation of the AAMs [Clausi et al. 2016].

SEM-EDS analyses confirm the amorphous structure of both LP10 and LP20 binders, with matrices appearing compact and dense. Some unreacted particles from the original precursor are still present, as confirmed also by XRD analyses (Supplementary Material 1 Figure S2). The elemental composition of the two binders, as determined by EDS is plotted on ternary phase diagrams of CaO-SiO_2-Al_2O_3 and SiO_2-Na_2O-Al_2O_3 (Supplementary Material 1 Figure S4 and Table S2 in supplementary material). Most of the points fall within the N-A-S-H region or the low Ca (C-(N)-A-S-H) region [van Deventer et al. 2014]. The chemical composition is comparable to that of alkali-activated volcanic ash [Djobo et al. 2016]. Increased Si and Al content provided by the higher amount of MK within the AAM mixtures leads to the increased formation of N-A-S-H gel, as seen in the case of the LP20 binder (Supplementary Material 1 Figure S4A, S4B).

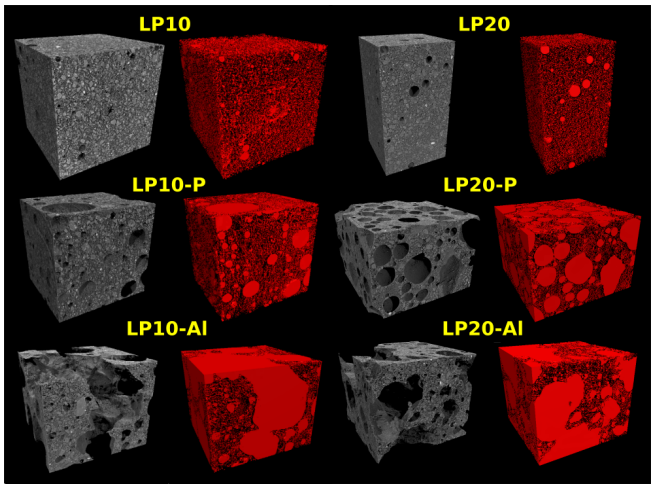

Figure 4: 3D renderings of the analysed Volume of Interest (VOIs) and related isosurface renderings of the extracted vesicle phase.

The release of OH^- and alkaline ions into water was assessed by measuring pH and electrical conductivity with the aim of testing the progression of the alkaline reaction. The electrical conductivity of the binders varied with a significant rate from 0 to 60 min and slowed down in the following hours (Supplementary Material 1 Figure S5). At minute zero the conductivity values of LP10 and LP20 were 171 and 88 µS cm^{-1}, respectively (electrical conductivity of the double-distilled water in which they were immersed = 1 µS cm^{-1}). After 1 hour, the values measured for LP10 became 5 times higher and for LP20 almost 7 times higher, reaching 856 and 588 µS cm^{-1}, respectively. After 24 hours, at the end of the measurement, LP10 showed an electrical conductivity of 2830 µS cm^{-1}, against 1154 µS cm^{-1} of LP20, two and a half times higher than the latter. Similar tests carried out using volcanic ash from Etna volcano, Italy, as additive for alkali activated materials showed an electrical conductivity ranging between 1000 to 10,000 µS cm^{-1} [Barone et al. 2021]. After introducing the samples into the water solution, pH values suddenly increased toward alkaline values from 7.2 to 10.45 (LP10) and 10.22 (LP20), subsequently remaining quite stable during the 24 hour-long test, reaching 10.58 for LP10 and 10.56 for LP20.

Porosity (ϕ), investigated via the analysis of microtomographic 3D images (Figure 4), is present in all samples. It ranges from 5.78–6.41 vol.% in binders to 23.68–51.39 vol.% when hydrogen peroxide (H_2O_2) is added and ϕ = 48.35–61.53 vol.% when using metallic aluminum (Figure 5 and Supplementary Material 1 Table S1). The volumes of single pores cover a wide range of sizes (from 10^{-8} to 1 mm^3) and their distribution differs from binders and foamy AAMs. In particular, the volume frequency distribution diagram (Figure 5) shows that the binders are quite similar, marked by a bi-modal distribution peaking at 10^{-6}–10^{-5} and 10^{-3} mm^3. Samples with H_2O_2 and metallic Al, on the contrary, show a shift of

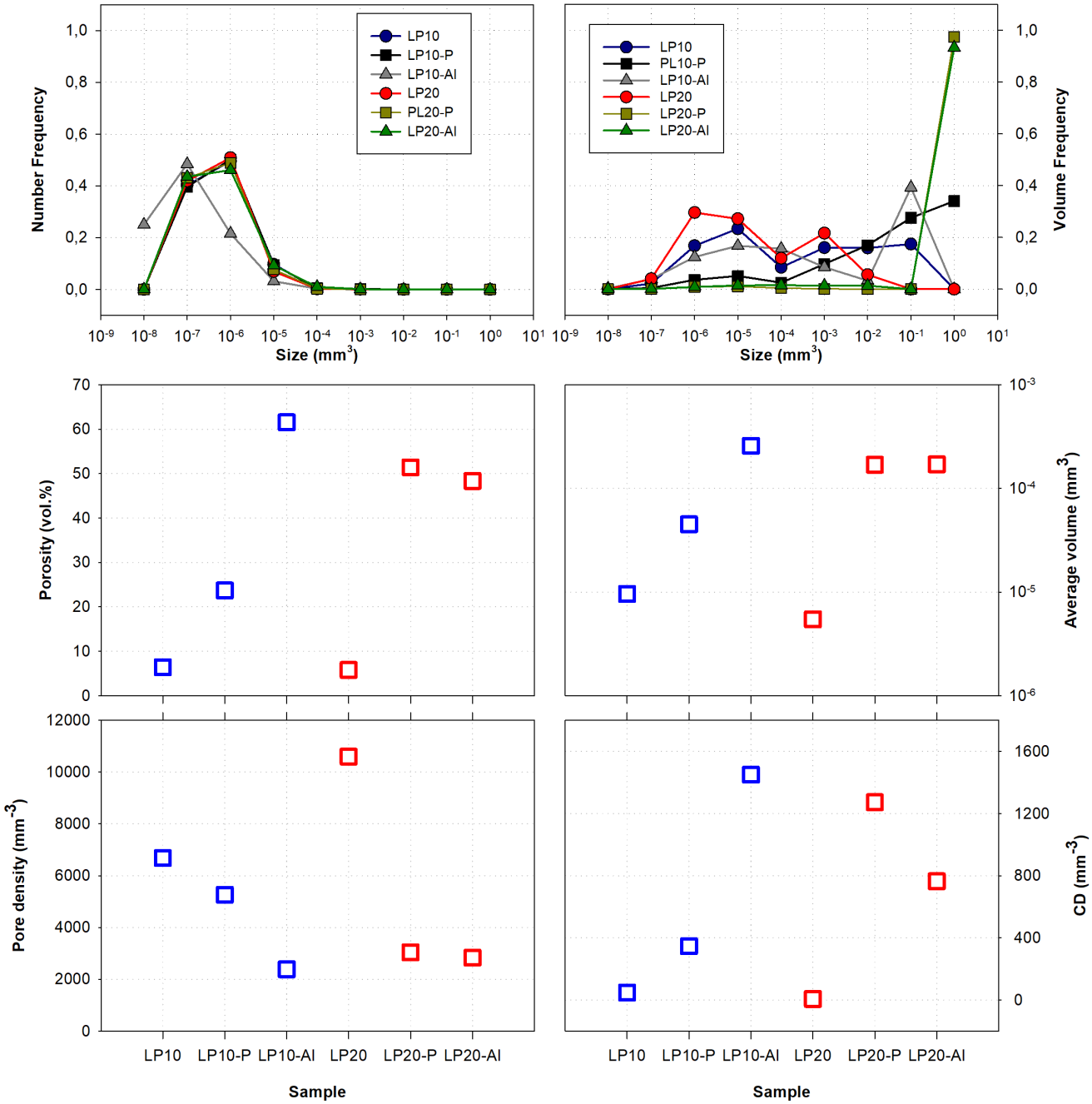

Figure 5: Results of the 3D image analysis of the pore phase showing the Number Frequency and Volume Frequency vs. Size distribution [see Lanzafame et al. 2020], and the values of porosity, average volume of each pore, pore density, and connectivity density for each sample.

the curves toward unimodal distributions peaking at 10^{-1} to 1 mm^3. Pore density (2800–10,500 mm^{-3}), average volume (5.4×10^{-6}–2.58×10^{-4} mm^3) and connectivity density (7–1149 mm^{-3}) are strictly correlated to each other, varying according to the total pore amount of the samples.

Results of flexural strength tests (Table 3) on the AAMs synthesized by using 10 wt.% of MK have comparable average values to their respective terms with 20 wt.% MK. LP10 and LP20 achieve 10.2 (± 0.3) MPa and 10.0 (± 1.6) MPa as average values, respectively. The uniaxial compressive strength test of four replicas for LP10 and LP20 (Table 3) display average values of 26.8 (± 2.5) MPa for LP10 and 27.7 (± 3.2) MPa for LP20. These results are comparable to C20/25 or C25/30 class of traditional concretes reported by Pucinotti [2013]. Following UNI EN 206-1: 2006, the two values indicate the minimum characteristic resistances, expressed in MPa, that a cylindric

Table 3: Results of flexural and compressive stress tests.

Test	Sample	Max stress (MPa)	Average (MPa)	St. Dev.*
Three points bending	LP10_1	10.3	10.15	0.28
	LP10_2	9.8		
	LP10_3	10.4		
	LP20_1	11.9	10.02	1.6
	LP20_2	9		
	LP20_3	9.2		
Uniaxial compressive strength	LP10_1	26.8	26.8	2.5
	LP10_2	26.8		
	LP10_3	23.6		
	LP10_4	29.8		
	LP20_1	25.7	27.7	3.2
	LP20_2	27.2		
	LP20_3	32.4		
	LP20_4	25.5		

* St. Dev. = standard deviation.

or a cubic specimen of concrete must bear, respectively. The trend of the stress-strain curves (Figure 6) shows small drops in stress as the strain increases, as recorded also for the same type of material by Occhipinti et al. [2020]. The two formulations differ only in terms of MK amounts, but the differences in terms of the average flexural and compressive strength are not relevant as reported in literature by Barone et al. [2020] and Occhipinti et al. [2023a]. These authors demonstrated a direct relationship between Etnean volcanic ash-based samples with 10 and 20 % of MK addition and resistance to mechanical stress.

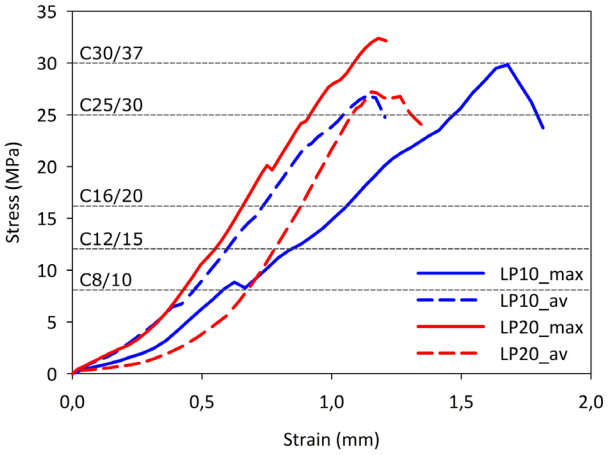

Figure 6: Uniaxial compressive strength of the samples: LP10 (blue lines) and LP20 (red lines). Solid lines indicate the maximum strength borne, while dashed lines indicate the average strength of the samples sets. Following UNI EN 206-1: 2006, reference uniaxial compressive strength of traditional concretes, reported by Pucinotti [2013] and referring to cubic specimens, are plotted as dark grey dashed lines.

4 Discussion

The synthesis of green alkali activated materials with mechanical properties matching the requirements for their use in building construction and restoration interventions is nowadays a well-established procedure that promises to speed up the ecological transition, involving the use of local materials and decreasing production costs. However, the challenge of this approach is to find the best balance between the number of raw materials, additives, and alkaline reagents and the curing temperature, which plays a crucial role in the energy demands of the entire productive process. Working at a temperature of > 40 °C assures good results, but partially hinders the aims of this technology. The main goal of this research is therefore to avoid any thermal curing treatment, obtaining products that can be synthesized directly on-site. Our first attempt to formulate AAMs using only Tajogaite ash and the alkaline activators at room temperature did not give satisfactory results since the materials did not harden. Based on these first results, a second set of AAMs was synthesized adding MK in amounts of 10 and 20 wt.% of the total of the solid, which guaranteed the development of both mechanical strength and chemical stability.

The use of MK also hindered the development of efflorescence that often forms in systems with only volcanic ash due to the low amount of Al^{-} which does not balance the Na^{+} from alkaline solution. In fact, the excess of Na^{+} in the gel system is often the cause of the formation of undesired soluble salts [Criado et al. 2005; Najafi Kani et al. 2012; Pacheco-Torgal et al. 2014], since it combines with atmospheric CO_2 leading to the formation of sodium carbonates that decrease the durability of the materials over time [Najafi Kani et al. 2012]. The absence of macroscopic efflorescence visible by the naked eye in all binders after 28 days of curing in air is encouraging and denotes chemical and mineralogical stability. Nevertheless, it appears from XRD, FTIR-ATR, and SEM-EDS analyses that only part of the ash had reacted under these con-

ditions and contributed to gel formation. This is evidenced by the slight increase in the amorphous amount within the AAMs (Table 2) and further corroborated by results of FTIR-ATR analysis (Supplementary Material 1 Figure S3). These results show changes in the shape and position of the main aluminosilicate band with respect to the original volcanic precursor due to both the contribution of the metakaolin in the mixtures (which forms the main band at 1034 cm^{-1}) and the reorganization of the molecular structure with the formation of aluminosilicate hydrate phases [Rees et al. 2007]. On the other hand, the unreacted fraction of ash acts as a filler, contributing to mechanical strength. The occurrence of the bands centered at 1263 cm^{-1} and at 795 cm^{-1} for LP10-Al, LP20-Al, and LP20-P can be attributed to the presence of aluminum in the first two, and to the higher quantity of metakaolin in the latter. Al and MK might affect the overall structure of the material, leading to an increase in Si–Al bonds and to a greater cross-linking of the gel network. Since MK is more reactive than volcanic glass, AAMs with 20 wt.% of MK benefit from a greater amount of aluminum and silicon than AAMs with 10 wt.% of MK. This leads to the appearance of bands linked to the bonds between silicon, aluminum and oxygen (Supplementary Material 1 Figure S3). An increase in Si–Al bonds is also shown by LP10-Al, but in this case, it can be attributed to the metallic aluminum used as a foaming agent for this specific sample. The presence of sodium carbonates, confirmed by XRD, FTIR analysis and electrical conductivity measurements, is lower in LP20 than in LP10 because of the higher amount (20 wt.%) of metakaolin used in LP20. This leads to a better stability of the polymeric structure in water, as confirmed by conductivity tests indicating a lower release of ions into the H_2O solution for LP20 with respect to LP10. The formation of the gel is also confirmed by SEM analyses, showing N-A-S-H gel as a first reaction product, with some areas from the original binders (LP10) to the porous samples obtained with hydrogen peroxide (LP10-P) and metallic aluminum (LP10-Al). The amount of metakaolin added (10 and 20 wt.%) had no impact on binder porosity (low for LP10 and LP20), whereas the use of H_2O_2 or metallic aluminum triggered foaming and led to very similar results in terms of pore amount, density, size, and volume distribution (Figure 5). In particular, the tendency to develop large pores in the LP20 porous samples is highlighted by the Volume Frequency diagram in Figure 5, showing that > 90% of the porosity is constituted by a small number of pores with larger sizes (1–10 mm^3). These results confirm the recent achievements of Occhipinti et al. [2023b] in the formulation of porous AAMs based on volcanic precursors: the pore phase can be tailored to obtain the desired amount of voids with a specific size. Porous materials are potentially attractive for a wide field of applications (e.g. thermal or acoustic insulation to water treatments and pH regulators). As an example, they may be useful in making the lightweight bricks widely employed on the island for plantations and gardens, in developing panels to be used for the reconstruction of some essential public buildings or in producing tiles for the finishes of new houses and apartments.

Previous authors have already performed feasibility studies making use of 2021 Tajogaite ash for the preparation of AAMs [Mañosa et al. 2023; Tashima et al. 2023]. In particular, Tashima et al. [2023] obtained good results in terms of workability and compressive strength (up to 95 MPa) for alkaline binders obtained using 8 mol kg^{-1} of Na^+ cured at 85 °C for up to 168 hours. Similarly, in the study of Mañosa et al. [2023], Tajogaite volcanic ash activated using 6 M NaOH is reported and shows a compressive strength of 16.5 MPa after 28 days of curing at temperature of 40–60 °C. In contrast to these studies, AAMs developed in this study were synthesized exclusively at room temperature, thanks to the addition of a small percentage of metakaolin that compensated for the low reactivity of the volcanic ash in the short timeframe, allowing faster hardening and the formation of the binding aluminosilicate gel. Room temperature curing is an essential condition for lowering both costs and energy demand related to the synthesis of the final products. In addition, the use of metakaolin meant a reduction in the use of industrial alkaline activators such as sodium silicate, which are the most expensive and energy demanding ingredients of the alkaline activation technology. Moreover, the use of non-pristine volcanic ash seems to be a good strategy, as early natural leaching allows the elimination of potentially dangerous components (S, Cl, Hg, Sb, As, etc. which pass to the hydrosphere [see e.g. Ruggieri et al. 2023]) in the raw materials and therefore in the AAM produced (for example, Mañosa et al. [2023] refer to the XRD detection of corderoite and fueloppite in their AAMs).

The use of volcanic ash from the island of La Palma (Spain) as a precursor in the alkali activation process allowed us to obtain innovative and sustainable materials that can be applied in both the construction and restoration fields. It is worth noting that Tajogaite products have mineral and chemical compositions typical of OIB volcanoes, with higher values of MgO and FeO compared to the common ash erupted by Etna volcano [Giacomoni et al. 2018; Viccaro et al. 2019; Giuffrida et al. 2023] which have already been successfully used in AAM production. For this reason, since OIB-related products occur in different areas of the globe and often represent the only natural resource locally available (as in the case of the volcanic island of La Palma), it is crucial to prioritize their use as raw materials as part of the green transition. The possible application of these materials is virtually infinite, and we encourage further studies aimed at discovering new applications for the recovery of La Palma.

5 Conclusions

A brief summary of the findings and significance of this work is reported below:

- The Tajogaite 2021 eruption ash can be efficiently used as precursor for the production of AAM binders with mechanical strength comparable to C20/25 or C25/30-class concrete (UNI EN 206 1:2006, see Figure 6), similar to those obtained from AAMs based on ash from Etna volcano, marking them as potential materials for construction and restoration purposes.

- The addition of a small percentage of metakaolin is crucial for formulating Tajogaite ash based-AAMs at room temperature. It enhances the reactivity of the ash in the alkaline activation process, reduces energy demand, and low-

ers CO_2 emissions in industrial production while maintaining high product performance.

- Pre-casted porous materials can be efficiently obtained chemically (i.e. by adding foaming agents such as hydrogen peroxide and metallic aluminum) which can be employed as lightweight monoliths or panels for industrial and environmental applications.

In conclusion, the results of this work demonstrate that the impact of disastrous eruptions such as the 2021 Tajogaite can be partially mitigated through the recovery and reuse of the huge volume of ash emitted, as part of the green transition. Instead of disposal, ash can be efficiently used as a raw material for AAM production in the reconstruction of public and private infrastructure. This would limit the costs related to the importation of traditional raw materials (e.g. cement) and favour a drastic cut in energy consumption related to the construction supply chain.

This work represents a first step toward the production of AAMs at room temperature using the 2021 Tajogaite volcanic products, and further studies are currently ongoing in order to improve the mechanical strength of the binders and better control the pore structure by varying the amount of foaming agents. The development of alkaline activation technology using OIB volcanic ash is of considerable significance. Indeed, such products are frequently emitted in volcanic areas that, despite being inhabited, are often situated in remote locations where the supply of raw materials involves high transportation costs. This offers a sustainable solution for regions where the efficient recycling of local resources can lead to both economic and ecological benefits.

Author Contributions

Roberta Occhipinti and Silvia Portale: Conceptualization, Fieldwork, AAMs formulation, Investigation, Data interpretation, Writing – original draft; Gabriele Lanzafame: Conceptualization, Fieldwork, Investigation, Data interpretation, Writing – original draft; Domingo Gimeno: Fieldwork, Investigation, Data interpretation, Writing – original draft; Marko Kudrna Prasek: Investigation, Data interpretation, Writing – original draft; Paolo Mazzoleni and Germana Barone: Conceptualization, Funding acquisition, Project administration, Resources, Supervision, Writing – original draft.

Acknowledgements

This research was supported by the following projects: The work of R.O., G.B. and P.M. was supported by MUR (Ministry of Education, Universities and Research of Italy) in the framework of PNRR Mission 4, Component 2, Investment 1.3 under project CHANGES, CUP E63C22001960006. The work of G.L. was supported by the Attraction and International Mobility (AIM1833071; CUP E66C18001310007); Fieldwork was supported by Pia.ce.ri. 2020-2022 Linea 2 – Progetto interdipartimentale SMOOCH (22722132152). D.G. was funded by Vicerectorate of Research of University of Barcelona. Although the sampling was carried out essentially outside the restricted area, we were able to access it and make interesting observations thanks to the involvement of Dr N. Pérez (INVOLCAN) and the permission provided by the representatives of the Autonomous Government of the Canary Islands. The authors acknowledge the personnel of the SYRMEP beamline of Elettra Synchrotron at Basovizza (Italy) for the precious help with the microtomography experiments, Kai Tandon and the Editor Ulrich Kueppers for the useful comments that helped to improve the quality and readability of the article and Alexander Bolam for his kind review of the English text.

Data Availability

All data supporting this research are available to readers upon request to the authors.

Copyright Notice

References

Aboulhassan, A., F. Brun, G. Kourousias, G. Lanzafame, M. Voltolini, A. Contillo, and L. Mancini (2022). "PyPore3D: An Open Source Software Tool for Imaging Data Processing and Analysis of Porous and Multiphase Media". *Journal of Imaging* 8(7), page 187. DOI: 10.3390/jimaging8070187.

Alzeer, M. I. M. and K. J. D. MacKenzie (2018). "Synthesis and Catalytic Properties of New Sustainable Aluminosilicate Heterogeneous Catalysts Derived from Fly Ash". *ACS Sustainable Chemistry amp; Engineering* 6(4), pages 5273–5282. DOI: 10.1021/acssuschemeng.7b04923.

Alzeer, M. I. M., K. J. D. MacKenzie, and R. A. Keyzers (2016). "Porous aluminosilicate inorganic polymers (geopolymers): a new class of environmentally benign heterogeneous solid acid catalysts". *Applied Catalysis A: General* 524, pages 173–181. DOI: 10.1016/j.apcata.2016.06.024.

Aulinas, M., D. Gimeno, J. Fernandez-Turiel, F. Perez-Torrado, A. Rodriguez-Gonzalez, and D. Gasperini (2010). "The Plio-Quaternary magmatic feeding system beneath Gran Canaria (Canary Islands, Spain): constraints from thermobarometric studies". *Journal of the Geological Society* 167(4), pages 785–801. DOI: 10.1144/0016-76492009-184.

Bai, C. and P. Colombo (2018). "Processing, properties and applications of highly porous geopolymers: A review". *Ceramics International* 44(14), pages 16103–16118. DOI: 10.1016/j.ceramint.2018.05.219.

Barbosa, V. F., K. J. MacKenzie, and C. Thaumaturgo (2000). "Synthesis and characterisation of materials based on inorganic polymers of alumina and silica: sodium polysialate polymers". *International Journal of Inorganic Materials* 2(4), pages 309–317. DOI: 10.1016/s1466-6049(00)00041-6.

Barone, G., M. C. Caggiani, A. Coccato, C. Finocchiaro, M. Fugazzotto, G. Lanzafame, R. Occhipinti, A. Stroscio, and P. Mazzoleni (2020). "Geopolymer production for conservation-restoration using Sicilian raw materials: fea-

sibility studies". *IOP Conference Series: Materials Science and Engineering* 777(1), page 012001. DOI: 10.1088/1757-899x/777/1/012001.

Barone, G., C. Finocchiaro, I. Lancellotti, C. Leonelli, P. Mazzoleni, C. Sgarlata, and A. Stroscio (2021). "Potentiality of the Use of Pyroclastic Volcanic Residues in the Production of Alkali Activated Material". *Waste and Biomass Valorization* 12(2), pages 1075–1094. DOI: 10.1007/s12649-020-01004-6.

Belaïd, F. (2022). "How does concrete and cement industry transformation contribute to mitigating climate change challenges?" *Resources, Conservation & Recycling Advances* 15, page 200084. DOI: 10.1016/j.rcradv.2022.200084.

Bernal, S. A., E. D. Rodríguez, A. P. Kirchheim, and J. L. Provis (2016). "Management and valorisation of wastes through use in producing alkali-activated cement materials". *Journal of Chemical Technology amp; Biotechnology* 91(9), pages 2365–2388. DOI: 10.1002/jctb.4927.

Bhuyan, M., R. Gebre, M. Finnilä, M. Illikainen, and T. Luukkonen (2022). "Preparation of filter by alkali activation of blast furnace slag and its application for dye removal". *Journal of Environmental Chemical Engineering* 10(1), page 107051. DOI: 10.1016/j.jece.2021.107051.

Brun, F., L. Mancini, P. Kasae, S. Favretto, D. Dreossi, and G. Tromba (2010). "Pore3D: A software library for quantitative analysis of porous media". *Nuclear Instruments and Methods in Physics Research Section A: Accelerators, Spectrometers, Detectors and Associated Equipment* 615(3), pages 326–332. DOI: 10.1016/j.nima.2010.02.063.

Brun, F., L. Massimi, M. Fratini, D. Dreossi, F. Billé, A. Accardo, R. Pugliese, and A. Cedola (2017). "SYRMEP Tomo Project: a graphical user interface for customizing CT reconstruction workflows". *Advanced Structural and Chemical Imaging* 3(1). DOI: 10.1186/s40679-016-0036-8.

Carracedo, J. C., V. R. Troll, J. M. D. Day, H. Geiger, M. Aulinas, V. Soler, F. M. Deegan, F. J. Perez-Torrado, G. Gisbert, E. Gazel, A. Rodriguez-Gonzalez, and H. Albert (2022). "The 2021 eruption of the Cumbre Vieja volcanic ridge on La Palma, Canary Islands". *Geology Today* 38(3), pages 94–107. DOI: 10.1111/gto.12388.

Castro, J. M. and Y. Feisel (2022). "Eruption of ultralow-viscosity basanite magma at Cumbre Vieja, La Palma, Canary Islands". *Nature Communications* 13(1). DOI: 10.1038/s41467-022-30905-4.

Civico, R., T. Ricci, P. Scarlato, J. Taddeucci, D. Andronico, E. Del Bello, L. D'Auria, P. A. Hernández, and N. M. Pérez (2022). "High-resolution Digital Surface Model of the 2021 eruption deposit of Cumbre Vieja volcano, La Palma, Spain". *Scientific Data* 9(1). DOI: 10.1038/s41597-022-01551-8.

Clausi, M. and D. Pinto (2023). "Valorisation of Water Potabilization Sludges as Precursors for Alkali-Activated Binders: Characterization and Feasibility Study". *Materials* 16(5), page 1998. DOI: 10.3390/ma16051998.

Clausi, M., S. C. Tarantino, L. L. Magnani, M. P. Riccardi, C. Tedeschi, and M. Zema (2016). "Metakaolin as a precursor of materials for applications in Cultural Heritage: Geopolymer-based mortars with ornamental stone aggregates". *Applied Clay Science* 132–133, pages 589–599. DOI: 10.1016/j.clay.2016.08.009.

Clayden, N., S. Esposito, A. Aronne, and P. Pernice (1999). "Solid state 27Al NMR and FTIR study of lanthanum aluminosilicate glasses". *Journal of Non-Crystalline Solids* 258(1–3), pages 11–19. DOI: 10.1016/s0022-3093(99)00555-4.

Cloetens, P., M. Pateyron-Salomé, J. Y. Buffière, G. Peix, J. Baruchel, F. Peyrin, and M. Schlenker (1997). "Observation of microstructure and damage in materials by phase sensitive radiography and tomography". *Journal of Applied Physics* 81(9), pages 5878–5886. DOI: 10.1063/1.364374.

Criado, M., A. Palomo, and A. Fernandez-Jimenez (2005). "Alkali activation of fly ashes. Part 1: Effect of curing conditions on the carbonation of the reaction products". *Fuel* 84(16), pages 2048–2054. DOI: 10.1016/j.fuel.2005.03.030.

Davidovits, J. (1991). "Geopolymers: Inorganic polymeric new materials". *Journal of Thermal Analysis* 37(8), pages 1633–1656. DOI: 10.1007/bf01912193.

Davidovits, J., L. Buzzi, P. Rocher, D. Gimeno, C. Marini, and S. Tocco (1999). "Geopolymeric cement based on low cost geologic materials. Results from the european research project geocistem". *Proceedings of the 2nd International Conference on Geopolymer*. Volume 99, pages 83–96.

Dingwell, D., Y. Lavallée, and U. Kueppers (2012). "Volcanic ash: A pri3y agent in the Earth system". *Physics and Chemistry of the Earth, Parts A/B/C* 45–46, pages 2–4. DOI: 10.1016/j.pce.2011.07.007.

Djobo, J. N. Y., A. Elimbi, H. K. Tchakouté, and S. Ku3 (2017). "Volcanic ash-based geopolymer cements/concretes: the current state of the art and perspectives". *Environmental Science and Pollution Research* 24(5), pages 4433–4446. DOI: 10.1007/s11356-016-8230-8.

Djobo, J. N. Y., H. K. Tchakouté, N. Ranjbar, A. Elimbi, L. N. Tchadjié, and D. Njopwouo (2016). "Gel Composition and Strength Properties of Alkali-Activated Oyster Shell-Volcanic Ash: Effect of Synthesis Conditions". *Journal of the American Ceramic Society* 99(9). Edited by J. Biernacki, pages 3159–3166. DOI: 10.1111/jace.14332.

Feng, J., R. Zhang, L. Gong, Y. Li, W. Cao, and X. Cheng (2015). "Development of porous fly ash-based geopolymer with low thermal conductivity". *Materials amp; Design (1980-2015)* 65, pages 529–533. DOI: 10.1016/j.matdes.2014.09.024.

Finocchiaro, C., G. Barone, P. Mazzoleni, C. Leonelli, A. Gharzouni, and S. Rossignol (2020). "FT-IR study of early stages of alkali activated materials based on pyroclastic deposits (Mt. Etna, Sicily, Italy) using two different alkaline solutions". *Construction and Building Materials* 262, page 120095. DOI: 10.1016/j.conbuildmat.2020.120095.

Finocchiaro, C., G. Barone, P. Mazzoleni, C. Sgarlata, I. Lancellotti, C. Leonelli, and M. Romagnoli (2021). "Artificial neural networks test for the prediction of chemical stability of pyroclastic deposits-based AAMs and comparison with conventional mathematical approach (MLR)". *Journal of Materials Science* 56(1), pages 513–527. DOI: 10.1007/s10853-020-05250-w.

Fletcher, R. A., K. J. MacKenzie, C. L. Nicholson, and S. Shimada (2005). "The composition range of aluminosilicate geopolymers". *Journal of the European Ceramic Society* 25(9), pages 1471–1477. DOI: 10.1016/j.jeurceramsoc.2004.06.001.

Fugazzotto, M., R. Occhipinti, M. C. Caggiani, A. Coccato, C. Finocchiaro, G. Lanzafame, P. Mazzoleni, G. Nucatolo, G. Piacenti, S. Starinieri, A. Stroscio, and G. Barone (2023). "Restoration feasibility study by using alkali activated mortars based on Mt. Etna volcanic ash: The case study of Monreale Cathedral (Palermo, Italy)". *Materials Letters* 333, page 133626. DOI: 10.1016/j.matlet.2022.133626.

Ge, Y., Y. Yuan, K. Wang, Y. He, and X. Cui (2015). "Preparation of geopolymer-based inorganic membrane for removing Ni2+ from wastewater". *Journal of Hazardous Materials* 299, pages 711–718. DOI: 10.1016/j.jhazmat.2015.08.006.

Giacomoni, P., M. Coltorti, S. Mollo, C. Ferlito, M. Braiato, and P. Scarlato (2018). "The 2011–2012 paroxysmal eruptions at Mt. Etna volcano: Insights on the vertically zoned plumbing system". *Journal of Volcanology and Geothermal Research* 349, pages 370–391. DOI: 10.1016/j.jvolgeores.2017.11.023.

Gimeno, D., J. Davidovits, C. Marini, P. Rocher, S. Tocco, S. Cara, N. Diaz, C. Segura, and G. Sistu (2003). "Desarrollo de un cemento de base silicatada a partir de rocas volcánicas vítreas alcalinas: interpretación de los resultados preindustriales basada en la composición químico-mineralógica de los precursores geológicos". *Boletín de la Sociedad Española de Cerámica y Vidrio* 42(2), pages 69–78. DOI: 10.3989/cyv.2003.v42.i2.643.

Gisbert, G. and D. Gimeno (2017). "Ignimbrite correlation using whole-rock geochemistry: an example from the Sulcis (SW Sardinia, Italy)". *Geological Magazine* 154(4), pages 740–756. DOI: 10.1017/s0016756816000327.

Giuffrida, M., M. Cardone, F. Zuccarello, and M. Viccaro (2023). "Etna 2011–2022: Discoveries from a 12ade of activity at the volcano". *Earth-Science Reviews* 245, page 104563. DOI: 10.1016/j.earscirev.2023.104563.

González-García, D., T. Boulesteix, A. Klügel, and F. Holtz (2023). "Bubble-enhanced basanite–tephrite mixing in the early stages of the Cumbre Vieja 2021 eruption, La Palma, Canary Islands". *Scientific Reports* 13(1). DOI: 10.1038/s41598-023-41595-3.

Gualtieri, A. and M. Zanni (1998). "Quantitative Determination of Crystalline and Amorphous Phase in Traditional Ceramics by Combined Rietveld-RIR Method". *Materials Science Forum* 278–281, pages 834–839. DOI: 10.4028/www.scientific.net/msf.278-281.834.

Hajimohammadi, A., T. Ngo, P. Mendis, and J. Sanjayan (2017). "Regulating the chemical foaming reaction to control the porosity of geopolymer foams". *Materials amp; Design* 120, pages 255–265. DOI: 10.1016/j.matdes.2017.02.026.

Horwell, C. J. and P. J. Baxter (2006). "The respiratory health hazards of volcanic ash: a review for volcanic risk mitigation". *Bulletin of Volcanology* 69(1), pages 1–24. DOI: 10.1007/s00445-006-0052-y.

Játiva, A., E. Ruales, and M. Etxeberria (2021). "Volcanic Ash as a Sustainable Binder Material: An Extensive Review". *Materials* 14(5), page 1302. DOI: 10.3390/ma14051302.

Lanzafame, G., F. Casetta, P. P. Giacomoni, S. Donato, L. Mancini, M. Coltorti, T. Ntaflos, and C. Ferlito (2020). "The Skaros effusive sequence at Santorini (Greece): Petrological and geochemical constraints on an interplinian cycle". *Lithos* 362–363, page 105504. DOI: 10.1016/j.lithos.2020.105504.

Le Maitre, R. W., editor (2002). *Igneous Rocks: A Classification and Glossary of Terms*. 2nd edition. Cambridge University Press. ISBN: 9780511535581. DOI: 10.1017/cbo9780511535581.

Lechler, P. and M. Desilets (1987). "A review of the use of loss on ignition as a measurement of total volatiles in whole-rock analysis". *Chemical Geology* 63(3–4), pages 341–344. DOI: 10.1016/0009-2541(87)90171-9.

Lemougna, P. N., A. Adediran, J. Yliniemi, T. Luukkonen, and M. Illikainen (2021). "Effect of organic resin in glass wool waste and curing temperature on the synthesis and properties of alkali-activated pastes". *Materials amp; Design* 212, page 110287. DOI: 10.1016/j.matdes.2021.110287.

Longpré, M.-A. (2021). "Reactivation of Cumbre Vieja volcano". *Science* 374(6572), pages 1197–1198. DOI: 10.1126/science.abm9423.

Luna-Galiano, Y., C. Leiva, C. Arenas, and C. Fernández-Pereira (2018). "Fly ash based geopolymeric foams using silica fume as pore generation agent. Physical, mechanical and acoustic properties". *Journal of Non-Crystalline Solids* 500, pages 196–204. DOI: 10.1016/j.jnoncrysol.2018.07.069.

Mañosa, J., J. Serrano-Conte, A. Maldonado-Alameda, M. Aulinas, and J. M. Chimenos (2023). "Pyroclastic volcanic ash as a potential precursor of alkali-activated binders – A case study from Tajogaite (La Palma, Canary Islands) volcano eruption". *Journal of Building Engineering* 72, page 106623. DOI: 10.1016/j.jobe.2023.106623.

Matinde, E. (2018). "Mining and metallurgical wastes: a review of recycling and re-use practices". *Journal of the Southern African Institute of Mining and Metallurgy* 118(8). DOI: 10.17159/2411-9717/2018/v118n8a5.

Najafi Kani, E., A. Allahverdi, and J. L. Provis (2012). "Efflorescence control in geopolymer binders based on natural pozzolan". *Cement and Concrete Composites* 34(1), pages 25–33. DOI: 10.1016/j.cemconcomp.2011.07.007.

Novais, R. M., T. Gameiro, J. Carvalheiras, M. P. Seabra, L. A. Tarelho, J. A. Labrincha, and I. Capela (2018). "High pH buffer capacity biomass fly ash-based geopolymer spheres to boost methane yield in anaerobic digestion". *Journal of Cleaner Production* 178, pages 258–267. DOI: 10.1016/j.jclepro.2018.01.033.

Novais, R. M., R. Pullar, and J. A. Labrincha (2020). "Geopolymer foams: An overview of recent advancements". *Progress in Materials Science* 109, page 100621. DOI: 10.1016/j.pmatsci.2019.100621.

Occhipinti, R., M. C. Caggiani, F. Andriulo, G. Barone, L. de Ferri, and P. Mazzoleni (2022). "Effect of atmospheric exposure on alkali activated binders and mortars from Mt. Etna volcanic precursors". *Materials Letters* 315, page 131940. DOI: 10.1016/j.matlet.2022.131940.

Occhipinti, R., M. C. Caggiani, L. de Ferri, Z. Xu, C. C. Steindal, N. Razavi, F. Andriulo, P. Mazzoleni, and G. Barone (2023a). "Structural properties of volcanic precursors-based geopolymers before and after natural weathering". *Ceramics International* 49(13), pages 21892–21902. DOI: 10.1016/j.ceramint.2023.04.013.

Occhipinti, R., A. M. Fernández-Jiménez, A. Palomo, S. C. Tarantino, and M. Zema (2021). "Sulfate-bearing clay and Pietra Serena sludge: Raw materials for the development of alkali activated binders". *Construction and Building Materials* 301, page 124030. DOI: 10.1016/j.conbuildmat.2021.124030.

Occhipinti, R., G. Lanzafame, A. Lluveras Tenorio, C. Finocchiaro, L. Gigli, M. R. Tinè, P. Mazzoleni, and G. Barone (2023b). "Design of alkali activated foamy binders from Sicilian volcanic precursors". *Ceramics International* 49(23), pages 38835–38846. DOI: 10.1016/j.ceramint.2023.09.220.

Occhipinti, R., A. Stroscio, C. Finocchiaro, M. Fugazzotto, C. Leonelli, M. José Lo Faro, B. Megna, G. Barone, and P. Mazzoleni (2020). "Alkali activated materials using pumice from the Aeolian Islands (Sicily, Italy) and their potentiality for cultural heritage applications: Preliminary study". *Construction and Building Materials* 259, page 120391. DOI: 10.1016/j.conbuildmat.2020.120391.

Pacheco-Torgal, F., J. Labrincha, C. Leonelli, A. Palomo, and P. Chindaprasit (2014). *Handbook of alkali-activated cements, mortars and concretes*. Elsevier. ISBN: 978-1-78242-276-1.

Paganin, D., S. C. Mayo, T. E. Gureyev, P. R. Miller, and S. W. Wilkins (2002). "Simultaneous phase and amplitude extraction from a single defocused image of a homogeneous object". *Journal of Microscopy* 206(1), pages 33–40. DOI: 10.1046/j.1365-2818.2002.01010.x.

Pankhurst, M. J., J. H. Scarrow, O. A. Barbee, J. Hickey, B. C. Coldwell, G. K. Rollinson, J. A. Rodríguez-Losada, A. Martín Lorenzo, F. Rodríguez, W. Hernández, D. Calvo Fernández, P. A. Hernández, and N. M. Pérez (2022). "Rapid response petrology for the opening eruptive phase of the 2021 Cumbre Vieja eruption, La Palma, Canary Islands". *Volcanica* 5(1), pages 1–10. DOI: 10.30909/vol.05.01.0110.

Pathak, A. K., T. Mukherjee, and D. K. Maity (2008). "IR Spectra of Carbonate-Water Clusters, CO3 2(H2O)n: A Theoretical Study". *Synthesis and Reactivity in Inorganic, Metal-Organic, and Nano-Metal Chemistry* 38(1), pages 76–83. DOI: 10.1080/15533170701854148.

Portale, S., C. Finocchiaro, R. Occhipinti, P. Mazzoleni, and G. Barone (2023). "Feasibility study about the use of basalt sawing sludge in building and restoration". *Materials Letters* 333, page 133624. DOI: 10.1016/j.matlet.2022.133624.

Provis, J. L. and J. S. J. van Deventer (2009). *Geopolymers: structures, processing, properties and industrial applications*. Elsevier. ISBN: 978-1-84569-449-4.

Pucinotti, R. (2013). "Assessment of in situ characteristic concrete strength". *Construction and Building Materials* 44, pages 63–73. DOI: 10.1016/j.conbuildmat.2013.02.041.

Razak, R. A., M. M. A. Abdullah, K. Hussin, K. N. Ismail, I. G. Sandu, D. Hardjito, Z. Yahya, and A. V. Sandu (2014). "Assessment on the potential of volcano ash as artificial lightweight aggregates using geopolymerisation method". *Revista de Chimie* 65, pages 828–834. DOI: 10.37358/Rev.Chim.1949.

Rees, C. A., J. L. Provis, G. C. Lukey, and J. S. J. van Deventer (2007). "Attenuated Total Reflectance Fourier Transform Infrared Analysis of Fly Ash Geopolymer Gel Aging". *Langmuir* 23(15), pages 8170–8179. DOI: 10.1021/la700713g.

Rickard, W. D. and A. van Riessen (2014). "Performance of solid and cellular structured fly ash geopolymers exposed to a simulated fire". *Cement and Concrete Composites* 48, pages 75–82. DOI: 10.1016/j.cemconcomp.2013.09.002.

Rickard, W. D., L. Vickers, and A. van Riessen (2013). "Performance of fibre reinforced, low density metakaolin geopolymers under simulated fire conditions". *Applied Clay Science* 73, pages 71–77. DOI: 10.1016/j.clay.2012.10.006.

Romero, J. E., D. Andronico, C. Bonadonna, J. Taddeucci, M. Pistolesi, M. Burton, M. Polacci, M. F. Rodríguez, A. Martín, P. Scarlato, H. C, and M. Pankhurst (2022a). "Volume and stratigraphy of the Cumbre Vieja 2021 eruption tephra fallout, La Palma Island". *Volcanic and Magmatic Studies Group annual meeting*. The University of Manchester, 10–12 January 2022.

Romero, J. E., M. Burton, F. Cáceres, J. Taddeucci, R. Civico, T. Ricci, M. J. Pankhurst, P. A. Hernández, C. Bonadonna, E. W. Llewellin, M. Pistolesi, M. Polacci, C. Solana, L. D'Auria, F. Arzilli, D. Andronico, F. Rodríguez, M. Asensio-Ramos, A. Martín-Lorenzo, C. Hayer, P. Scarlato, and N. M. Perez (2022b). "The initial phase of the 2021 Cumbre Vieja ridge eruption (Canary Islands): Products and dynamics controlling edifice growth and collapse". *Journal of Volcanology and Geothermal Research* 431, page 107642. DOI: 10.1016/j.jvolgeores.2022.107642.

Rowles, M. and B. O'Connor (2003). "Chemical optimisation of the compressive strength of aluminosilicate geopolymers synthesised by sodium silicate activation of metakaolinite". *Journal of Materials Chemistry* 13(5), pages 1161–1165. DOI: 10.1039/b212629j.

Ruggieri, F., G. Forte, B. Bocca, B. Casentini, A. Bruna Petrangeli, A. Salatino, and D. Gimeno (2023). "Potentially harmful elements released by volcanic ash of the 2021 Tajogaite eruption (Cumbre Vieja, La Palma Island, Spain): Implications for human health". *Science of The Total Environment* 905, page 167103. DOI: 10.1016/j.scitotenv.2023.167103.

Schindelin, J., I. Arganda-Carreras, E. Frise, V. Kaynig, M. Longair, T. Pietzsch, S. Preibisch, C. Rueden, S. Saalfeld, B. Schmid, J.-Y. Tinevez, D. J. White, V. Hartenstein, K. Eliceiri, P. Tomancak, and A. Cardona (2012). "Fiji: an open-source platform for biological-image analysis". *Nature Methods* 9(7), pages 676–682. DOI: 10.1038/nmeth.2019.

Shi, K., B. Yu, Y. Zhou, Y. Chen, C. Yang, Z. Chen, and J. Wu (2019). "Spatiotemporal variations of CO2 emissions and their impact factors in China: A comparative analysis between the provincial and prefectural levels". *Applied Energy* 233–234, pages 170–181. DOI: 10.1016/j.apenergy.2018.10.050.

Sitarz, M., M. Handke, and W. Mozgawa (2000). "Identification of silicooxygen rings in SiO2 based on IR spectra". *Spectrochimica Acta Part A: Molecular and Biomolecular Spectroscopy* 56(9), pages 1819–1823. DOI: 10.1016/s1386-1425(00)00241-9.

Stewart, C., D. Johnston, G. Leonard, C. Horwell, T. Thordarson, and S. Cronin (2006). "Contamination of water supplies by volcanic ashfall: A literature review and simple impact modelling". *Journal of Volcanology and Geothermal Research* 158(3–4), pages 296–306. DOI: 10.1016/j.jvolgeores.2006.07.002.

Tashima, M. M., L. Soriano, M. V. Borrachero, J. Monzó, and J. Payá (2023). "Towards the valorization of Cumbre Vieja volcanic ash – Production of alternative cements". *Construction and Building Materials* 370, page 130635. DOI: 10.1016/j.conbuildmat.2023.130635.

Taylor, W. R. (1990). "Application of infrared spectroscopy to studies of silicate glass structure: Examples from the melilite glasses and the systems Na2O-SiO2 and Na2O-Al2O3-SiO2". *Journal of Earth System Science* 99(1), pages 99–117. DOI: 10.1007/bf02871899.

Tchakoute, H., A. Elimbi, E. Yanne, and C. D1gang (2013). "Utilization of volcanic ashes for the production of geopolymers cured at ambient temperature". *Cement and Concrete Composites* 38, pages 75–81. DOI: 10.1016/j.cemconcomp.2013.03.010.

Tchakoute Kouamo, H., A. Elimbi, J. Mbey, C. Ngally Sabouang, and D. Njopwouo (2012). "The effect of adding alumina-oxide to metakaolin and volcanic ash on geopolymer products: A comparative study". *Construction and Building Materials* 35, pages 960–969. DOI: 10.1016/j.conbuildmat.2012.04.023.

van Deventer, J. S. J., R. San Nicolas, I. Ismail, S. A. Bernal, D. G. Brice, and J. L. Provis (2014). "Microstructure and durability of alkali-activated materials as key parameters for standardization". *Journal of Sustainable Cement-Based Materials* 4(2), pages 116–128. DOI: 10.1080/21650373.2014.979265.

Viccaro, M., M. Giuffrida, F. Zuccarello, M. Scandura, M. Palano, and S. Gresta (2019). "Violent paroxysmal activity drives self-feeding magma replenishment at Mt. Etna". *Scientific Reports* 9(1). DOI: 10.1038/s41598-019-43211-9.

Vitola, L., D. Bajare, A. Palomo, and A. Fernandez-Jimenez (2020). "Low-Calcium, Porous, Alkali-Activated Materials as Novel pH Stabilizers for Water Media". *Minerals* 10(11), page 935. DOI: 10.3390/min10110935.

Zhang, X., C. Bai, Y. Qiao, X. Wang, D. Jia, H. Li, and P. Colombo (2021). "Porous geopolymer composites: A review". *Composites Part A: Applied Science and Manufacturing* 150, page 106629. DOI: 10.1016/j.compositesa.2021.106629.

Zhang, Z., J. L. Provis, A. Reid, and H. Wang (2015). "Mechanical, thermal insulation, thermal resistance and acoustic absorption properties of geopolymer foam concrete". *Cement and Concrete Composites* 62, pages 97–105. DOI: 10.1016/j.cemconcomp.2015.03.013.